JGR Space Physics

RESEARCH ARTICLE
10.1029/2023JA031295

Key Points:

- Upstream and downstream waves at a low-Mach number quasi-parallel shock are investigated by 2-D hybrid simulations
- Upstream quasi-parallel and quasi-perpendicular waves are excited by the interaction of injected flow and backstreaming ions
- Downstream waves are generated by the mode conversion of upstream waves

Correspondence to:
Y. Hao,
yfhao@pmo.ac.cn

Citation:
Hao, Y., Lu, Q., Wu, D., & Xiang, L. (2023). Wave activities throughout a low-Mach number quasi-parallel shock: 2-D hybrid simulations. *Journal of Geophysical Research: Space Physics*, *128*, e2023JA031295. https://doi.org/10.1029/2023JA031295

Received 6 JAN 2023
Accepted 3 MAY 2023

Wave Activities Throughout a Low-Mach Number Quasi-Parallel Shock: 2-D Hybrid Simulations

Yufei Hao[1,2,3], Quanming Lu[2,3], Dejin Wu[1], and Liang Xiang[1,4]

[1]Key Laboratory of Planetary Sciences, Purple Mountain Observatory, Chinese Academy of Sciences, Nanjing, China, [2]CAS Key Laboratory of Geospace Environment, Department of Geophysics and Planetary Science, University of Science and Technology of China, Hefei, China, [3]Collaborative Innovation Center of Astronautical Science and Technology, Hefei, China, [4]Institute of Space Physics, Luoyang Normal University, Luoyang, People's Republic of China

Abstract In this paper, two-dimensional hybrid simulations are used to study wave excitation and evolution throughout a low-Mach number quasi-parallel shock. Simulation results show that quasi-parallel fast magnetosonic waves, ion Bernstein waves with harmonics and possible Alfven/ion cyclotron waves can be excited in the upstream region, and their small phase velocities compared to injected flow velocity results in the convection to the shock front where they are mode converted into several groups of downstream waves, including Alfven waves along the directions parallel to downstream average magnetic fields and perpendicular to the shock normal, the quasi-perpendicular kinetic slow waves and possible kinetic Alfven waves. We suggest that downstream Alfven waves originate from the mode conversion of upstream quasi-parallel fast magnetosonic waves with left-hand polarization in the downstream rest frame under helicity conservation, while the downstream left-hand polarized kinetic slow waves and right-hand polarized kinetic Alfven waves can be from the upstream quasi-perpendicular ion Bernstein waves.

1. Introduction

Collisionless shocks are ubiquitous and always thought to be important sources of power-law spectra of the nonthermal components detected by energetic particle collectors from space and astrophysical plasma (Jones & Ellison, 1991). At quasi-perpendicular shocks, which have a larger shock angle ($\theta_{\mathrm{Bn}} > 45°$) defined as the angle between shock normal and upstream background magnetic field, reflected particles at the shock front can quickly gyrate back and be accelerated by shock surfing acceleration and shock drifting acceleration mechanisms in the direction perpendicular to the background magnetic field (Lembege et al., 2004; Mckean et al., 1996; Yang et al., 2012; Zank et al., 2006), which leads to large perpendicular temperature anisotropy in the immediately downstream and resultant excitation of ion cyclotron waves and mirror waves (S. P. Gary, 1992; S. P. Gary et al., 1976, 1994). And, the directly transmitted particles behind the quasi-perpendicular shock front can also provide the free energy to drive these ion anisotropy instabilities by their bunched ring-like distributions (Gedalin, 2016; Gedalin et al., 2016; Y. Hao et al., 2014; Lee, 2017; Lee & Lee, 2016; Q. M. Lu & Wang, 2005, 2006).

At a quasi-parallel shock with $\theta_{\mathrm{Bn}} < 45°$ under medium and high Mach numbers, reflected particles after being initially accelerated near the shock front can backstream to further upstream and interact with the injected flow (Burgess, 1989; Cao et al., 2009; Hao, Lembege, et al., 2016; Jarvinen et al., 2020; Kajdič et al., 2021; Pfau-Kempf et al., 2015, 2016, 2018; Lin, 2003; Lin & Wang, 2005; Scholer & Terasawa, 1990; Su, Lu, Gao, et al., 2012; Su, Lu, Hunag, et al., 2012; Turc et al., 2018). It leads to the excitation of right-hand resonant electromagnetic ion beam instabilities and generates low-frequency quasi-parallel propagating fast magnetosonic waves (S. P. Gary, 1991), which can always be observed at terrestrial foreshock region and named 30s waves or ultra-low-frequency (ULF) waves (Eastwood et al., 2002; Palmroth et al., 2015; Wang et al., 2020; Wilson, 2016) whose phase velocities and group velocities inherently point to further upstream in the rest plasma frame (Otsuka et al., 2019). While, under these Mach numbers injected flow with large bulk velocity can wash them into the shock front and make it to be unstable (Krauss-Varban & Omidi, 1993), such that cyclic reformation processes happen in a so-called extended turbulent region where particles also behave periodically as the upstream waves continuously disturb the shock front (Burgess, 1989; Scholer & Burgess, 1992; Su, Lu, Gao, et al., 2012; Su, Lu, Hunag, et al., 2012; Thomas et al., 1990; Turc et al., 2022).

Under low Alfven Mach numbers Omidi et al. (1990) substantiate that quasi-parallel shocks show a stable state and a narrow transition region with a distinct ramp where high-frequency whistler waves can be radiated with a nearly zero group velocity in the shock frame of reference, so that they always stay around the shock front and are called phase-standing whistlers (Kan & Swift, 1983; Kennel et al., 1984a, 1984b; Mandt et al., 1986; Quest et al., 1983; Scholer & Fujimoto, 1993; Thomsen et al., 1993). Most of energy fluxes of these waves cannot be convected back and disturb the shock front as at a high Mach one, so that it shows steady behaviors and has a relatively clean downstream region. Krauss-Varban and Omidi (1991) suggest that with 1-D hybrid simulations, quasi-parallel shocks with a sufficiently small Alfven Mach number, e. g., $M_A < 2.3$ as $\theta_{\mathrm{Bn}} = 30°$, show the stable state, and as increasing the Mach number, upstream waves begin to be convected back and bring the unsteadiness of shock fronts till $M_A = 2.8$ under which a typical cyclically reformed process can be distinguished with sufficient energy flux of these shock-directed waves.

Recently, with a 2-D hybrid simulation code Y. Q. Hao et al. (2021) studied upstream low-frequency waves at a quasi-parallel shock with typical parameters around the terrestrial bow shock (Burgess, 1989; Burgess et al., 2005), and found shell-like distributions originating from the superthermal backstreaming components (Winske & Leroy, 1984), quasi-parallel and quasi-perpendicular propagating fast magnetosonic waves excited by both of these two nonequilibrium distributions in whole upstream region (P. S. Gary, 1985; P. S. Gary et al., 1984; S. Gary et al., 1981; S. P. Gary & Tokar, 1985; Min & Liu, 2015a, 2015b; Sun et al., 2016a, 2016b). And, they all can be brought back to the shock front to facilitate its renewal (Burgess, 1989; Y. Hao et al., 2017; Scholer & Fujimoto, 1993), intermittent reflected particles and directly transmitted high-speed flow (Han et al., 2016, 2017; Hao, Lembege, et al., 2016, Hao, Lu, Gao, & Wang, 2016; Hietala et al., 2009, 2012; Palmroth et al., 2021; Plaschke et al., 2018). In the downstream, after being transmitted through the shock front these upstream waves are mode converted into the proposed Alfven waves and slow waves (Krauss-Varban & Omidi, 1991, 1993), which eventually are heavily damped except for the quasi-perpendicular kinetic slow waves (KSWs) (Y. X. Hao et al., 2018; Narita & Marsch, 2015). Under this Mach number condition, substantial upstream wave energy flux are convected back so that in the so-called transition region are many nonlinear structures like new shock fronts and downstream large scale belt-like structures (Y. Hao et al., 2017), which may mask the wave information (Scholer & Fujimoto, 1993; Scholer et al., 1997). In this paper, for a quasi-parallel shock with a proper low Mach number we perform 2-D hybrid simulations to investigate all the possible waves in its upstream and downstream.

In Section 2 of this paper, we describe the details of the 2-D hybrid simulation model and the associated parameters. In Section 3, simulation results are presented. Conclusions and discussion are given in the last section.

2. Simulation Model

A 2-D hybrid simulation code is used to study the waves around a low Mach number quasi-parallel shock in this paper. The simulation is performed in $x - y$ plane where the background magnetic field lies in, and the simulation code has rigid boundaries in x direction and periodic boundaries in y direction. At the beginning, there are 30 particles in each cell, and after it running, a magnetized plasma with a Maxwellian velocity distribution begin to be continuously injected from left boundary. Then, the right moving plasma is reflected by the right boundary and interact with the continuously injected flow, which leads to the formation of a shock front propagating to the $-x$ direction. For each time step, information of particles are collected and used to update the electromagnetic fields by Maxwell's equations and the equation of state of electrons, and then they push particles to obtain updated velocity components and positions (Hao, Lu, et al., 2016).

The bulk velocity of injected flow is $2.0V_A$ (where V_A is the upstream Alfven speed), and propagating velocity of the shock is about $0.8V_A$, which means the Alfven Mach number of the shock is 2.8. The shock angle is set to be 30°, and upstream plasma beta is $\beta_i = \beta_e = 0.4$ (where i and e indicate protons and electrons, respectively). Simulations use an electron resistivity length $L_\eta = \eta c^2/(4\pi V_A) = 0.1c/\omega_{\mathrm{pi}}$, where $\eta/4\pi = 1.1 \times 10^{-5}\omega_{\mathrm{pi}}^{-1}$ describes the wave-particle interaction resulting from high frequency plasma instabilities associated with electron mass as in Leroy et al. (1981, 1982). The grid sizes Δx is $0.5c/\omega_{\mathrm{pi}}$ and Δy is $1.0c/\omega_{\mathrm{pi}}$, so the grid cells are smaller in x direction than they are in y direction to show more microstructures in the direction of shock normal (Krauss-Varban & Omidi, 1993; Scholer & Fujimoto, 1993), which leads to a simulation area with length $L_x = n_x \times \Delta x = 1000 \times 0.5c/\omega_{\mathrm{pi}} = 500c/\omega_{\mathrm{pi}}$ and width $L_y = n_y \times \Delta y = 300 \times 1.0c/\omega_{\mathrm{pi}} = 300c/\omega_{\mathrm{pi}}$ (where n_x, n_y, are the numbers of grid cell in the x, y directions, and c and ω_{pi} denote the speed of light and ion plasma frequency). The time step is $\Omega_i \Delta t = 0.02$ (where Ω_i is the ion gyrofrequency).

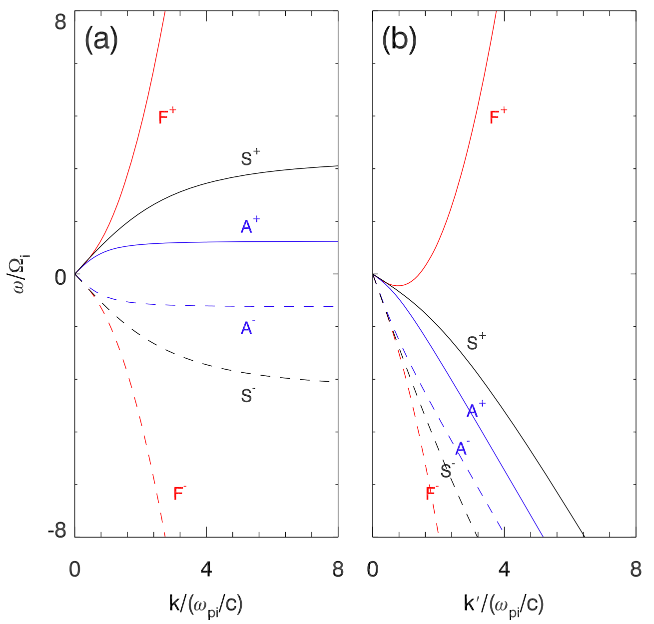

Figure 1. Dispersions from a two-fluid plasma theory with thermal correction in (a) the plasma frame and (b) downstream rest frame. F^+, A^+, and S^+ indicate the upstream-directed fast magnetosonic-whistler wave, Alfven/ion cyclotron wave and ion-sound wave branches, while F^-, A^- and S^- denote the corresponding downstream-directed wave branches in the plasma frame.

3. Simulation Results

3.1. Upstream Waves and Associated Ion Dynamics

To analyze the waves around the quasi-parallel shock, a simplified and relatively accurate dispersion relation is necessary for a warm plasma. That of the fast magnetosonic/whistler (F) waves and Alfven/ion cyclotron (A) waves can be derived by the cold two-fluid theory, and after adding finite kinetic thermal correction it may describe more modes, including slow/ion acoustic (S) waves and kinetic Alfven waves (KAWs) (Yoon & Fang, 2008). In Figure 1a, the corrected dispersion relations of upstream-directed F^+, S^+, A^+ waves and downstream-directed F^-, S^-, A^- waves are depicted with solid and dashed lines in different colors when $\beta_i = \beta_e = 0.4$, and it shows that the phase speed of S mode can be larger than F mode under low frequency condition and even as higher frequency it is always larger than A mode (Krauss-Varban et al., 1994).

Simulations in the paper, however, are performed in the downstream rest frame, the dispersion relations should take into account the Doppler shift when analyzing the wave information from simulation data (Y. Q. Hao et al., 2023). Therefore, in Figure 1b we display the shifted dispersion relations for upstream waves

$$\omega(k)/\Omega_{\rm pi} = k\left(c/\omega_{\rm pi}\right)\cdot\left(v_{\rm ph}(V_A) - V_{\rm inj}\cos(\theta_{\rm Bn})(V_A)\right)$$

where ω, k, and $v_{\rm ph}$ are the frequencies, wave vectors and corresponding phase velocities, respectively. We can see that phase speeds and group velocities of most of wave modes point to downstream except for high-frequency F^+ waves, which means that substantial wave energy flux can be brought into the shock front to affect the evolution of structures, ion dynamics around the shock front and even wave activities in the downstream region. Throughout this paper, the corrected dispersions with and without Doppler shift will be used to detect the plasma waves generated in the upstream and downstream, where the plasma has a larger beta. And, note that the strongly damped S mode should not be excited in the region before the shock front (S. P. Gary, 1992).

In Figure 2, we illustrate the contour plots of variations of (a) $\delta b_z/B_0$ and (b) $\delta N/N_0$ in the upstream region at time $\Omega_i t = 188.5$ when the shock front at $x = 353c/\omega_{\rm pi}$ is denoted by a vertical black dashed line, and the other two lines labeled $L1$ and $L2$ are parallel and perpendicular to the upstream background magnetic field $\mathbf{B_0}$. From Figure 2a, we can see regular waveforms with wave fronts nearly perpendicular to $\mathbf{B_0}$, which suggests possible existence of quasi-parallel propagating electromagnetic waves. That should be the well-known low-frequency

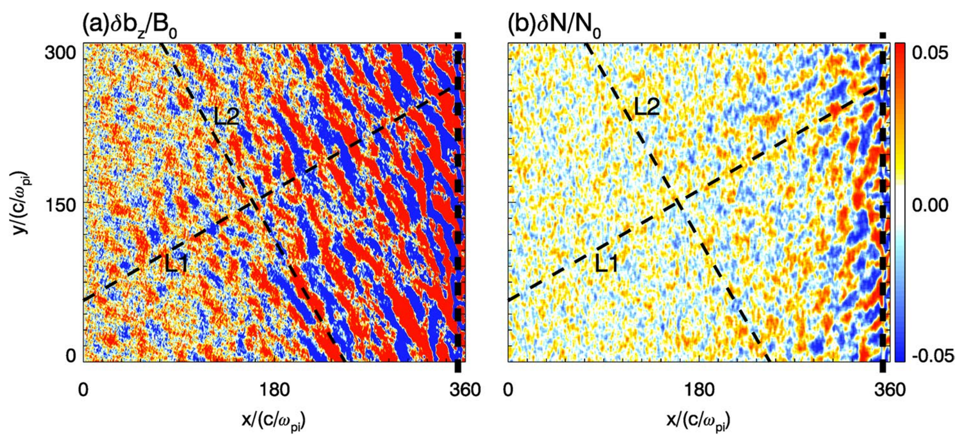

Figure 2. Contour plots of (a) $\delta b_z/B_0$ and (b) $\delta N/N_0$ in the upstream region. The shock front at $x = 353c/\omega_{\rm pi}$ is denoted by a black dashed line. Line $L1$ and $L2$ are respectively parallel and perpendicular to the background magnetic fields.

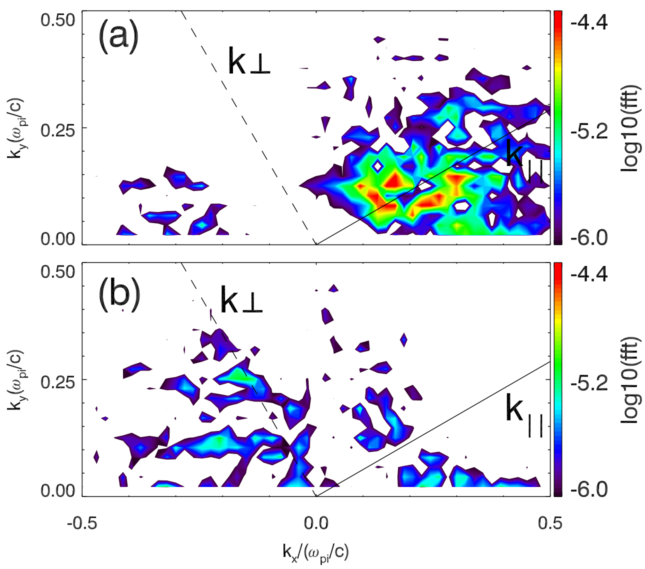

Figure 3. Wave power spectra of the variations in Figure 2 in an area ($10 < x < 345c/\omega_{\rm pi}$; $0 < y < 300c/\omega_{\rm pi}$).

fast magnetosonic waves driven by the interaction between the backstreaming particles and injected flow (S. P. Gary, 1991; Y. Q. Hao et al., 2021) or the ULF waves shown by experiment data from space missions in terrestrial or planetary foreshocks (Burgess et al., 2005; Hoppe & Russell, 1982; Shan et al., 2016). While, from variations of particle number density in Figure 2b the possible wave fronts are mainly parallel to $\mathbf{B_0}$ and their intensity is lower compared to that in Figure 2a. And, these variations may also be due to the quasi-perpendicular fast magnetosonic waves as discussed in previous work under a medium Alfven Mach number (Y. Q. Hao et al., 2021).

To confirm the intuition about these upstream waves, Figure 3 illustrates the power spectra of these variations, $\delta b_z/B_0$ and $\delta N/N_0$, in an upstream area ($10 < x < 345c/\omega_{\rm pi}$; $0 < y < 300c/\omega_{\rm pi}$), and $k_\parallel$, $k_\perp$ are indicated by black solid and dashed lines, respectively. The main modes are highlighted by white color to mask the regions with much lower values, which is also employed for power spectra plots in the following. In Figure 3a, quasi-parallel waves can be clearly seen and they have a higher intensity compared to the quasi-perpendicular waves shown in Figure 3b. At a medium Alfven Mach number quasi-parallel shock (Y. Q. Hao et al., 2021), upstream quasi-perpendicular waves can have nearly equal or higher intensity compared to the quasi-parallel ones, which may result from more backstreaming particles with a higher temperature and enough free energy to excite quasi-perpendicular waves (S. Gary et al., 1981).

Along the line $L1$ and $L2$, the simulation data of the variations of $\delta b_z/B_0$ and $\delta N/N_0$ is respectively collected from the time $\Omega_i t = 100$ to $\Omega_i t = 188$ in bins of $0.5c/\omega_{\rm pi}$ and $0.1\Omega_i^{-1}$. Figure 4 displays the corresponding spectrograms, and dispersions of the transformed F^+, A^+, F^- and A^- modes are also plotted to analyze possible wave modes in the upstream region. In Figure 4a, where power spectrum of waves propagating in the direction of $\mathbf{B_0}$ the low-frequency part ($k_{//} < 1.0\omega_{\rm pi}/c$) with the largest intensity is well consistent to the F^+ mode dispersion, which should be the low-frequency resonant fast magnetosonic waves propagating in the same direction as bulk velocity of the beam by the prediction of linear theory (P. S. Gary et al., 1984; S. Gary et al., 1981; S. P. Gary & Tokar, 1985). And, it seems that low-frequency Alfven waves corresponding to A^+ mode are also excited by the left-hand resonant ion beam instabilities because of the backstreaming superthermal particles (P. S. Gary et al., 1984), which also had been predicted by kinetic linear theory using a general dispersion relation solver PDRK (Y. Q. Hao et al., 2021; Xie, 2019; Xie & Xiao, 2016). In addition, high-frequency waves ($k_{//} > 1.0\omega_{\rm pi}/c$) are generated and their spectrogram is consistent to all of these four modes, including upstream-directed F^+ mode, downstream-directed F^-, Alfven/ion cyclotron mode A^+ and A^- (Min & Liu, 2015a, 2015b; Sun et al., 2016a, 2016b), which is thought to be excited by the shell-like or ring-like distributions originating from backstreaming particles being scattered by upstream low-frequency waves (Y. Q. Hao et al., 2021; Winske & Leroy, 1984).

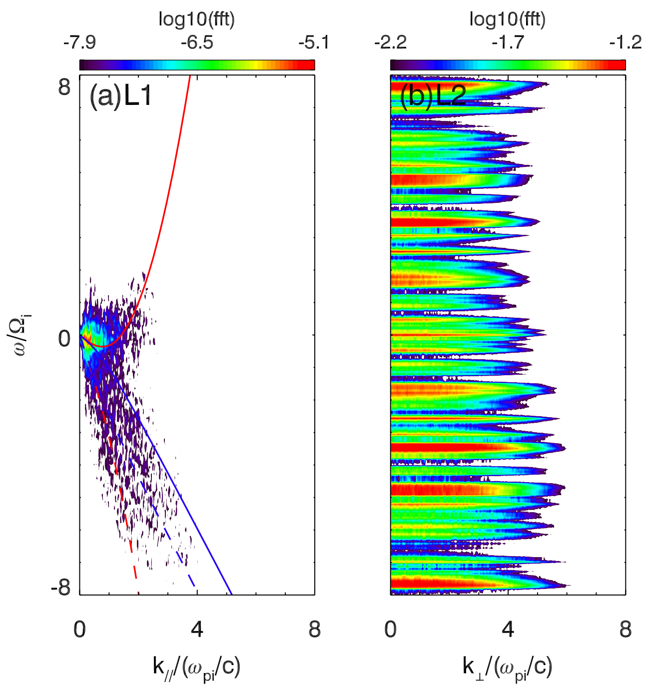

Figure 4. Spectrograms of (a) $\delta b_z/B_0$ along line $L1$ and (b) $\delta N/N_0$ along line $L2$ from the time $\Omega_i t = 100$ to $\Omega_i t = 188$ in bins of $0.5c/\omega_{\rm pi}$ and $0.1\Omega_i^{-1}$.

Waves associated with the ring-distributions are well studied by linear theory and simulations (Min & Liu, 2015a, 2015b; Sun et al., 2016a, 2016b), which suggest that kinetic instabilities can be driven to generate quasi-parallel ion cyclotron waves, oblique mirror waves and ion Bernstein waves. That may not only explain the high-frequency F and A modes propagating along the line $L1$, but also further demonstrate that the quasi-perpendicular fast magnetosonic waves, which had been detected at a medium Alfven Mach number shock (Y. Q. Hao et al., 2021), are also excited and show harmonics as shown in Figure 4b where spectrogram of the variations of $\delta N/N_0$ along line $L2$ is illustrated. It should be noted that the discrete structures in Figure 4b can be

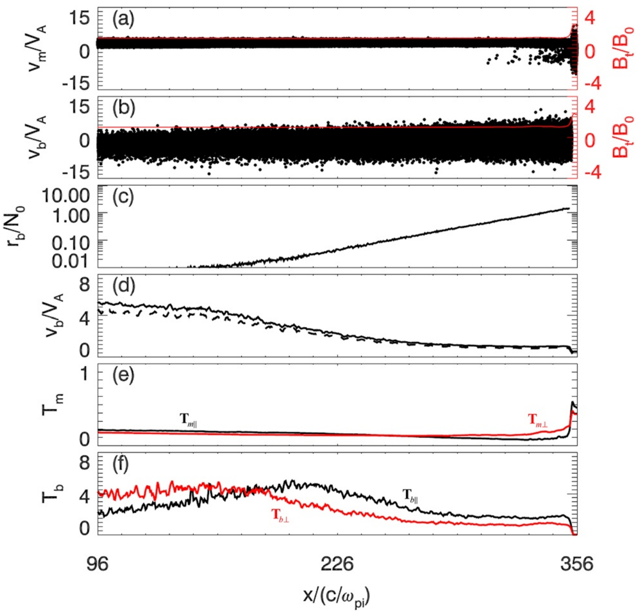

Figure 5. From top to bottom: (a) ion phase space of injected particles; (b) ion phase space of backstreaming particles; (c) the ratio of backstreaming particles to injected flow; (d) the relative drift velocities between backstreaming and injected flows in the directions of shock normal and background magnetic fields indicated by black solid and dashed lines, respectively; (e) the perpendicular temperature $T_{m\perp}$ and parallel temperature $T_{m\parallel}$ of injected particles indicated by red and black lines, respectively; (f) the temperatures of backstreaming particles as (e).

also due to the discrete nature of positive wave growth rate of ion cyclotron waves excited by the ring-like distributions, and the associated mirror waves might be excited with a comparable low growth rate and resultant lower intensity so that it is difficult to identify them in the upstream region (Min & Liu, 2015a, 2015b).

In Figure 5, for all of the particles in the simulation plane we display ion phase plot $x - v_{ix}$ of (a) the injected particles and (b) backstreaming ions with the total magnetic fields denoted by red solid lines for reference. Figure 5c illustrates the ratio of backstreaming ions to injected particles, and their relative drift velocities in the directions of shock normal and $\mathbf{B_0}$ are plotted with black solid and dashed lines in Figure 5d. The perpendicular and parallel temperatures of injected particles and backstreaming ions are shown in Figures 5e and 5f with red and black solid lines, respectively. We can see that from Figure 5a, thermal velocity of these particles seems to have a visible enhancements behind the shock front, and just before it few thermalized particles have not been grouped into the backstreaming particles shown in the second panel. In Figure 5b, these backstreaming particles are observably hotter than the injected particles because these particles usually backstream from the shock front after their initial energization (Hao, Lu, et al., 2016; Scholer, 1990; Su, Lu, Gao, et al., 2012). And, their particle number density in Figure 5c has an exponential increase when approaching the shock front, which had also been suggested by 1-D hybrid simulations (Scholer, 1993). In Figure 5d, the relative drift velocities in both directions show very similar values, and they are larger in further upstream than in immediate upstream region, where more backstreaming particles tend to be scattered back to the shock front by higher intensity of waves so that the bulk velocity pointing to upstream is lower (Hao, Lu, et al., 2016). Therefore, we can imagine that left-hand resonant ion beam instabilities generate Alfven/ion cyclotron waves due to the lower relative drift velocity and these waves lead to $T_{m\perp} > T_{m\parallel}$ and $T_{b\parallel} > T_{b\perp}$ in the upstream region close to the shock front as shown in Figures 5e and 5f, while in further upstream region large relative drift velocity tends to drive low-frequency right-hand resonant fast magnetosonic waves that results in $T_{b\parallel} < T_{b\perp}$, which had been proved by linear and second-order theory (P. S. Gary, 1985; S. P. Gary & Tokar, 1985).

3.2. Analysis of Downstream Waves

Previous studies had suggested that upstream waves convected by injected flow can be mode converted into downstream Alfven waves and slow waves (Krauss-Varban, 1995; Krauss-Varban & Omidi, 1991, 1993), which are heavily damped so that just KSWs can be easily found (Y. X. Hao et al., 2018). Here, we further investigate the downstream waves under the large spatial and temporal scales of a low Mach number quasi-parallel shock, which may have fewer nonlinear structures around the shock front. Therefore, waves can be easily seen by the variations of associated physical quantities and detected by Fourier transforming them and the proposed two-fluid dispersion relations with thermal correction (Yoon & Fang, 2008). In Figure 6, we show three components of downstream magnetic fields, and the position of the shock front is also indicated by black dashed lines at $x = 353c/\omega_{\mathrm{pi}}$. The dashed lines $L3$ and $L4$ parallel and perpendicular to the downstream average magnetic field are plotted and will be used to collect data of these variations associated to the parallel and perpendicular waves. From Figure 6a, we can see that the wave fronts are nearly parallel to the x axis, which means that there are waves propagating in the y direction. While, the contour plots of δb_y and δb_z show wave fronts lying in the direction nearly perpendicular to the downstream average magnetic fields. That is, in the downstream region are two groups of low-frequency waves that possibly originate from mode conversion of upstream waves, especially wave fronts in Figures 6b and 6c are nearly connected with that in upstream and lie in the same directions (not shown here). It reminds us of the suggestion that after mode conversion the helicities of upstream waves remain the same for downstream waves (Krauss-Varban & Omidi, 1991).

In Figure 7, we display the power spectra of these three components of magnetic fields in a downstream region ($360c/\omega_{\mathrm{pi}} < x < 495c/\omega_{\mathrm{pi}}$; $0c/\omega_{\mathrm{pi}} < y < 300c/\omega_{\mathrm{pi}}$) with $k_\parallel$ and $k_\perp$ denoted by black solid and dashed lines.

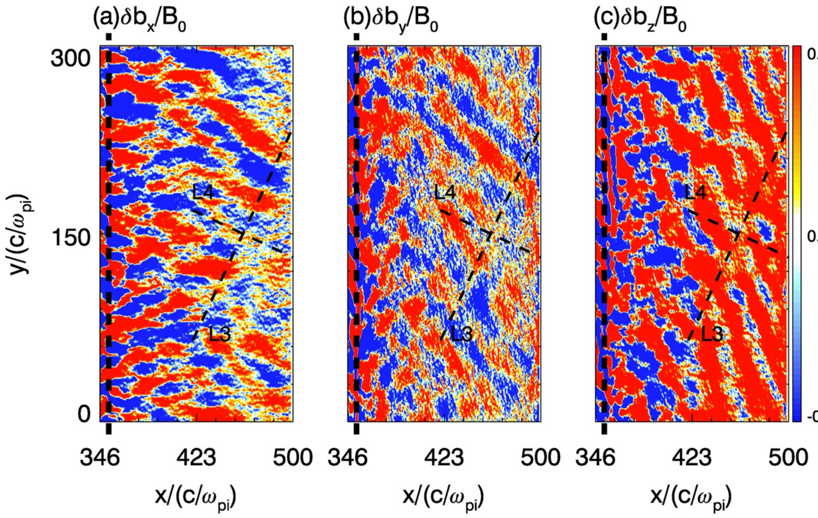

Figure 6. Contour plots of variations of the three magnetic field components: (a) $\delta b_x/B_0$, (b) $\delta b_y/B_0$, and (c) $\delta b_z/B_0$ in the downstream region. The shock front at $x = 353c/\omega_{\rm pi}$ is denoted with a black dashed line. Line $L3$ and $L4$ are, respectively, parallel and perpendicular to the downstream average magnetic fields.

The spectrogram of δb_x in Figure 7a suggests the low-frequency waves propagate along the y direction, which is consistent with the nearly horizontal wave fronts in Figure 6a. That of δb_y shows the quasi-parallel waves in Figure 7b, while for the δb_z its spectrogram indicates that there are waves propagating in the y direction and quasi-parallel waves with larger intensity compared to δb_y. It suggests that both of these two groups of low-frequency waves may be circularly polarized and should be oblique and quasi-parallel left-hand Alfven waves with weak compressibility (S. P. Gary, 1986), which can be found from the variations of particle number density and corresponding power spectrum (not shown here).

Similarly, to further investigate these downstream waves we collect the associated simulation data in the y direction at $x = 440c/\omega_{\rm pi}$ and along the lines $L3$, $L4$ in the same bins as in Figures 4, and Figure 8 illustrates their spectrograms of (a) δb_x in the y direction, (b) δb_y and (c) δN along $L3$, (d) δN along $L4$ with corresponding dispersion relations, which also come from the two-fluid theory with thermal correction under downstream $\beta_i = 0.97$ and are indicated by solid and dashed red (F), blue (A) and black (S) lines. It can be found that from Figure 8a, there are oblique Alfven waves and they are actually the waves propagating in the y direction as shown in Figures 6 and 7. And, their intensity as $k_y < 0$ is much larger than that of $k_y > 0$, which is similar to the suggestions at a perpendicular shock (Q. Lu et al., 2009; McKenzie & Westphal, 1969). Figure 8b shows the quasi-parallel Alfven waves, while the spectrogram in Figure 8c has no unambiguous implications because downstream Alfven waves as the origination of compressibility do not strictly propagate in the direction parallel to the average magnetic fields. In the perpendicular direction, in Figure 8d the possible waves have zero frequency and their intensity spreads around the quasi-perpendicular KSW and KAW dispersions, which are very close to each other. Although previous evidences under a medium Mach number quasi-parallel shock suggest the existence of KSWs, we cannot insist on the absences of KAWs in the downstream region due to their similarity of characterizations (J. S. Zhao et al., 2014).

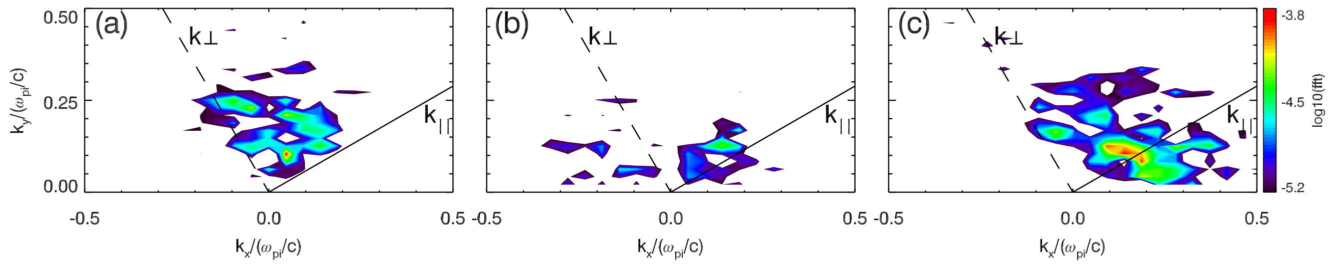

Figure 7. Wave power spectra of variations in Figure 6 in an area ($360c/\omega_{\rm pi} < x < 495c/\omega_{\rm pi}$; $0 < y < 300c/\omega_{\rm pi}$).

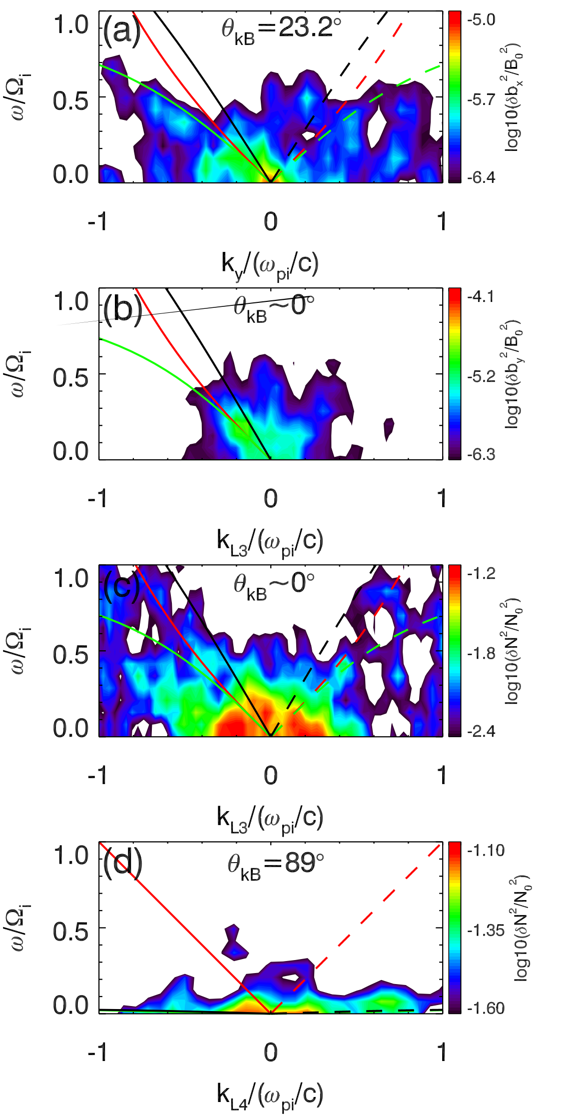

Figure 8. Spectrograms of (a) $\delta b_x/B_0$ along a line in the y direction at $x = 440c/\omega_{pi}$, (b) $\delta b_y/B_0$ along the line $L3$, (c) $\delta N/N_0$ along the line $L3$ and (d) $\delta N/N_0$ along the line $L4$ from the time $\Omega_i t = 100$ to $\Omega_i t = 188$ in bins of $0.5c/\omega_{pi}$ and $0.1\Omega_i^{-1}$.

In Figure 9, we display the temporal evolution of (a) $\delta b_x/B_0$, (b) $\delta b_z/B_0$, and (c) $\delta N/N_0$ in the y direction at $x = 440c/\omega_{pi}$. The time evolution of $\delta b_x/B_0$, which comes from the oblique Alfven waves propagating in the y direction as shown in Figures 6a and 7a, shows the forward and backward propagating wave modes, and obviously, the intensity of the forward propagating waves is several times that of the backward ones. That is consistent with the implications of Figure 8a and can be the clear evidence that upstream low-frequency fast magnetosonic waves undergo similar processes as at a perpendicular shock (Q. Lu et al., 2009; McKenzie & Westphal, 1969). Figure 9b just shows the forward propagating waves, which are actually the dominant quasi-parallel Alfven waves as shown in Figures 6c and 7c. The fluctuations of particles number density in Figure 9c are non-propagating KSWs and possible KAWs with zero frequency as shown in Figure 8d.

3.3. Overview of the Waves From Upstream to Downstream

At this low Mach number quasi-parallel shock, upstream quasi-parallel and quasi-perpendicular fast magnetosonic waves, which had been detected at a medium Mach one, can also be clearly found in the upstream region, though the quasi-perpendicular waves are relatively weak in amplitude. These waves, especially in the perpendicular direction, may bring compressibility and result in the upstream fluctuating total magnetic fields as shown in Figure 10a (S. P. Gary, 1986), while the dominant quasi-parallel waves close to the shock lead to strong transverse fluctuations and less compressibility as shown in Figures 10b and 10d (Y. Q. Hao et al., 2021). In the immediately downstream, from Figures 10a and 10d we can see highly compressive magnetic structures, which lie nearly along the downstream average magnetic fields and might be the large-scale belt-like structures proposed by Y. Hao et al. (2017). In further downstream region, there are oblique, quasi-parallel Alfven waves, very weak KSWs and possible KAWs, which bring reasonable stronger compressive magnetic fluctuations, negative cross helicity and relatively strong compressibility from top to bottom in Figure 10 (S. P. Gary & Winske, 1992; Y. X. Hao et al., 2018; J. S. Zhao et al., 2014). Meanwhile, the compression ratio between downstream and upstream as shown in Figure 10a is around 2, which is distinctly lower than the value derived by ideal magnetohydrodynamics (MHD) theory. That should be due to the very low Mach number of this simulated shock.

In the shock front, the upstream low-frequency quasi-parallel and quasi-perpendicular waves are mode converted into several groups of downstream waves. For the upstream quasi-parallel low-frequency waves, they are fast magnetosonic waves with right-hand circularly polarization (S. P. Gary, 1986) and become left-hand polarized in the downstream rest frame after Doppler shift. In Figure 11a, their corresponding dispersion is indicated by a red solid line, which is close to the dispersion relations of downstream eigenmodes denoted by dashed lines under the corresponding the simulated downstream $\beta = 0.97$. And, the spectrogram of upstream quasi-parallel waves is sketched by a gray shaded region, which covers all these three downstream plasma dispersions. While, taking into account the left-hand polarization of the upstream quasi-parallel low-frequency waves, it is reasonable that after their mode conversion, we should find quasi-parallel or oblique Alfven and slow waves, both of which are also left-hand polarized under the downstream plasma conditions (J. Zhao, 2015).

For the upstream waves in perpendicular direction, their phase speeds point to further upstream (uF^+) and the shock front (uF^-), and have right-hand elliptic polarizations with very small ellipticities in the plasma frame (S. P. Gary, 1986; Y. Q. Hao et al., 2021). Similarly, they can also be convected to the shock front due to their low phase speeds even down to zero (Y. Q. Hao et al., 2021), which leads to the reversal of polarization of uF^+. Therefore, in the downstream rest frame these quasi-perpendicular waves have left-hand and right-hand elliptic

10.1029/2023JA031295

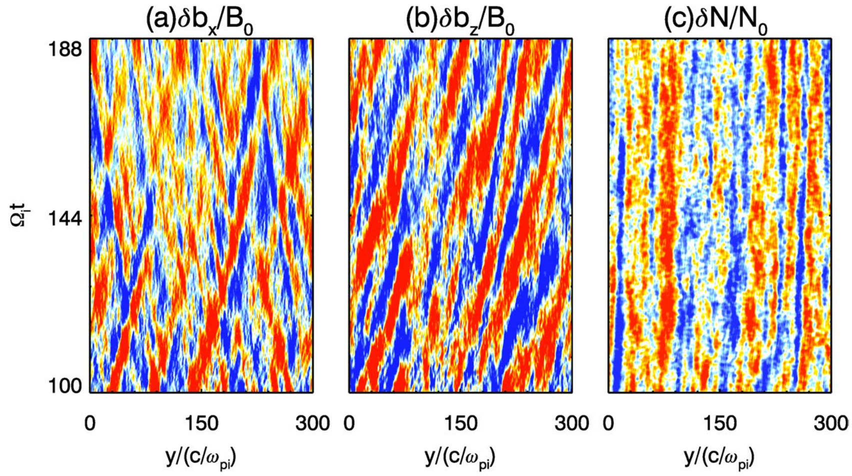

Figure 9. The dispersions of the two-fluid plasma theory with thermal correction are displayed under downstream plasma conditions and corresponding propagating angles θ_{kB}. F, A and S modes are plotted by red, yellow, and black lines.

polarizations. In Figure 11b, we display their sketches of spectrograms and corresponding dispersions of uF^{+} and uF^{-} denoted by red bold solid and dashed lines, respectively. And, downstream dispersions of dS^{+}, dS^{-}, dA^{+}, and dA^{-}, which are actually KSWs and KAWs in perpendicular direction, can be clearly distinguished and are very close to that of uF^{+}. While, note that all these dispersions are actually very close to each other if we plot them in the $(\omega, k_{\perp})$ with a large range of the y axis as Figure 4, even the dispersion of uF^{-} seems to be parallel to the x axis. Therefore, the upstream left-hand uF^{+} and right-hand uF^{-} in the downstream rest frame have a reasonable chance to be mode converted into downstream quasi-perpendicular left-hand KSWs and right-hand KAWs (S. P. Gary, 1986; Y. X. Hao et al., 2018; J. Zhao, 2015; J. S. Zhao et al., 2014), respectively. That is, not only KSWs but also KAWs can exist in the low Mach number quasi-parallel shocks, which is thought to be true under a higher Mach number, though only the existence of KSWs are evidenced in the downstream of a quasi-parallel shock with a medium Alfven Mach number (Y. X. Hao et al., 2018).

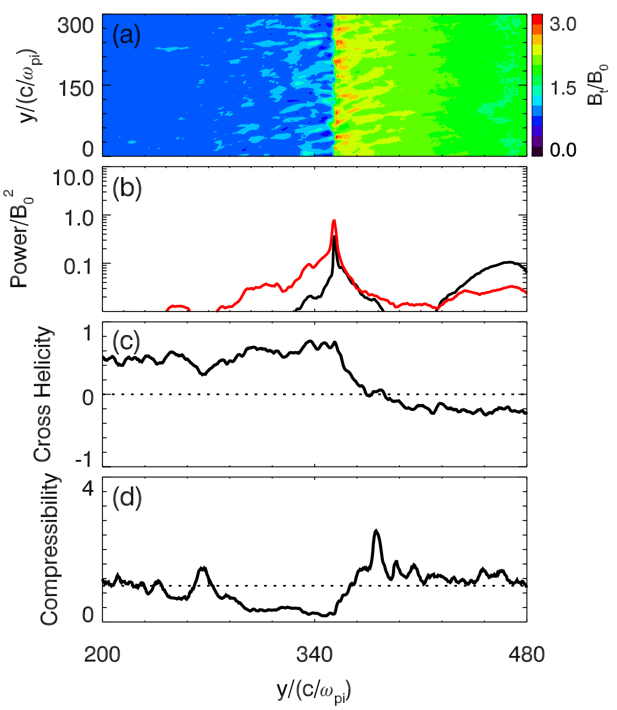

Figure 10. From top to bottom: (a) contour plot of the total magnetic fields in simulation plane; (b) transverse and compressive fluctuations denoted by red and black lines; (c) cross helicity; (d) compressibility.

As a summary, we illustrate a sketch of power spectrum of all the upstream and downstream waves in Figure 12. In the upstream region, there are quasi-parallel low frequency fast magnetosonic waves, Alfven/ion cyclotron waves and quasi-perpendicular ion Bernstein waves, which are labeled 1, 2, 3 in Figure 12a. The waves 1 result from the right-hand resonant electromagnetic ion beam instabilities driven by the interaction of backstreaming particles and injected flow, while wave 2 and 3 should be due to the shell-like or ring-like distributions of the backstreaming particles as suggestion in previous work (Y. Q. Hao et al., 2021). At the quasi-parallel shock front, waves 1 are mode converted into downstream quasi-parallel Alfven waves $1'$, Alfven waves $2'$ in y direction and oblique slow waves, which are heavily damped and are not shown in Figure 12b. Downstream quasi-perpendicular waves $3'$ should include two groups: KSWs and KAWs, and they are generated by the mode conversion of upstream quasi-perpendicular left-hand and right-hand elliptically polarized ion Bernstein waves 3 in the downstream rest frame, respectively.

4. Conclusions and Discussion

In this paper, we use a 2-D hybrid simulation code to investigate the waves at a low Mach number quasi-parallel shock. The simulation results suggest that except for the well-known low-frequency quasi-parallel fast magnetosonic waves, high-frequency Alfven/ion cyclotron waves and quasi-perpendicular

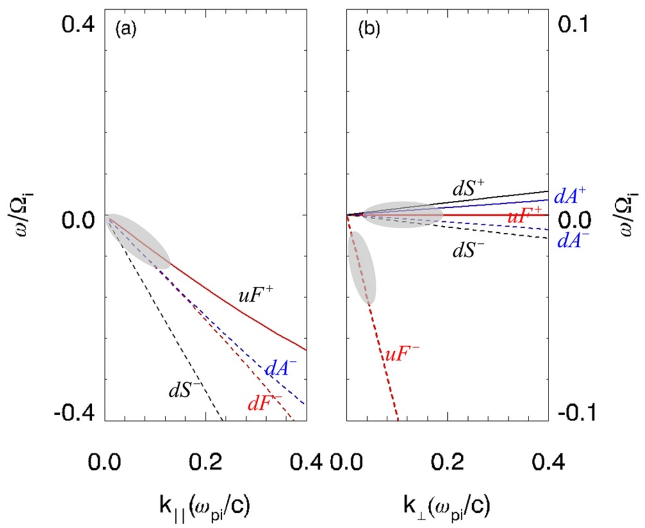

Figure 11. (a) The dispersion under upstream conditions uF^+ and downstream dispersions dF^-, dA^-, and dS^- in parallel direction. (b) The dispersions under upstream conditions uF^+ and uF^-, and downstream dispersions dA^+, dA^-, dS^+, and dS^-. The gray shaded regions denote the sketches of spectrograms of possible waves excited by the free energy from backstreaming particles.

ion Bernstein waves in the form of harmonics can also be generated by the backstreaming particles in upstream region. The quasi-parallel and quasi-perpendicular waves all can be brought back to the shock front where mode conversion happens and causes them to become Alfven waves propagating along the downstream average magnetic fields and the direction perpendicular to the shock normal, quasi-perpendicular KSWs and KAWs in the downstream region, respectively. These downstream and upstream waves are examined by a two-fluid plasma model with finite thermal correction.

Waves at a quasi-parallel shock always catch our attention due to their important role on the evolutions of associated ion dynamics and structures (Burgess et al., 2005). Shocks with medium and high Mach numbers can generate upstream waves with high intensity (Burgess, 1989; Y. Q. Hao et al., 2021; Scholer & Burgess, 1992), and these waves can steepen and become nonlinear structures as they are brought toward the shock front (Y. Hao et al., 2017; Scholer, 1993; Scholer & Fujimoto, 1993), even the waves and structures can have significant effects on the downstream (Y. X. Hao et al., 2018; Krauss-Varban & Omidi, 1991). At a very low Mach number one the excited upstream waves have phase speed pointing to upstream in the downstream rest frame and become phase-standing waves just before the shock front (Krauss-Varban & Omidi, 1991; Omidi et al., 1990), which leads to a stable shock front and a very clean downstream region. Here, under a proper Mach number we can clearly identify the upstream and downstream waves with little effect from nonlinear structures, and found more wave modes and their possible relationship throughout the shock front.

For mode conversion of the upstream waves at a quasi-parallel shock, it first requires that these waves can be convected back (Krauss-Varban & Omidi, 1991), that is, their group velocities should point to the shock front in the downstream rest frame to finally reach the region where wave mode conversion can happen (Shi et al., 2013). Therefore, the Alfven Mach numbers should exceed a threshold, e. g., $M_A = 2.3$ as $\theta_{\mathrm{Bn}} = 30°$, under which most of upstream waves begin to be brought back to the shock front. At the same time, the upstream waves have high frequency and large phase velocities under low Alfven Mach numbers (Blanco-Cano et al., 2016; Krauss-Varban & Omidi, 1993), so that the mode conversion requires a high compression ratio under the Alfven resonance condition $\omega^2 = k_\parallel^2 V_A^2 \left(1 - \omega^2/\Omega_i^2\right)^2$ (Lin et al., 2012). While, for the upstream waves excited at a medium and high Mach number shock, they are comparatively low-frequency and their phase velocities are around $\omega/k_\parallel = 2.0V_A$. And, in shock front the local Alfven velocities are around the same value, so the mode conversion of upstream

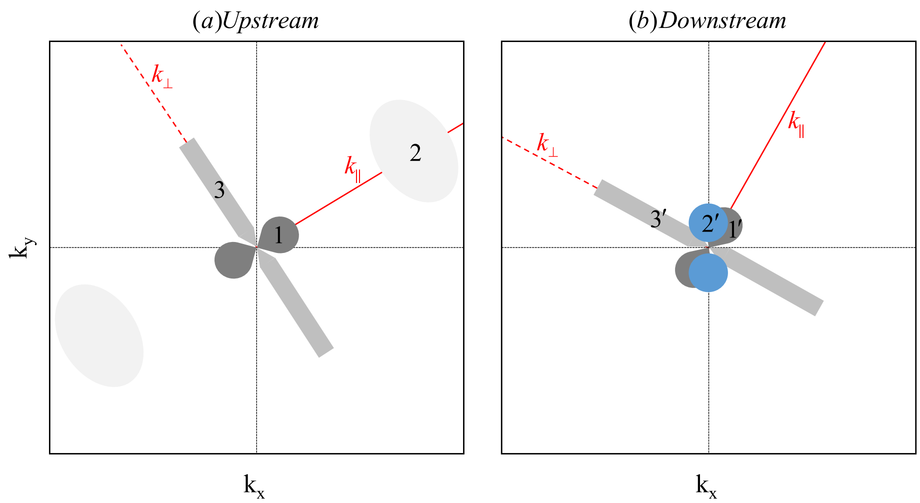

Figure 12. The sketches of power spectra of (a) upstream waves and (b) downstream waves.

waves should easily happen in some medium and high Mach number space environments, such as the terrestrial bow shock (Burgess et al., 2005; Zhang et al., 2022) and co-rotating interaction regions (Gosling & Pizzo, 1999; Jian et al., 2006; Kilpua et al., 2017; Richardson, 2018).

Data Availability Statement

Simulation data sets for this research are available at the following link https://doi.org/10.5281/zenodo.7725025.

Acknowledgments

This work was supported by NSFC Grants 41804158, 41531071, 11873018, and 11790302, National Key R&D Program of China E2GK111110 (2022YFF0503002), the Specialized Research Fund for State Key Laboratories, and Key Laboratory of Geospace Environment, University of Science and Technology of China.

References

Blanco-Cano, X., Kajdic, P., Aguilar-Rodriguez, E., Russell, C. T., Jian, L. K., & Luhmann, J. G. (2016). Interplanetary shocks and foreshocks observed by stereo during 2007-2010. *Journal of Geophysical Research: Space Physics*, *121*(2), 992–1008. https://doi.org/10.1002/2015JA021645

Burgess, D. (1989). Cyclic behavior at quasi-parallel collisionless shocks. *Geophysical Research Letters*, *16*(5), 345–348. https://doi.org/10.1029/GL016i005p00345

Burgess, D., Lucek, E. A., Scholer, M., Bale, S. D., Balikhin, M. A., Balogh, A., et al. (2005). Quasi-parallel shock structure and processes. *Space Science Reviews*, *118*(1–4), 205–222. https://doi.org/10.1007/s11214-005-3832-3

Cao, J. B., Fu, H. S., Zhang, T. L., Reme, H., Dandouras, I., & Lucek, E. (2009). Direct evidence of solar wind deceleration in the foreshock of the Earth. *Journal of Geophysical Research*, *114*(A2), A02207. https://doi.org/10.1029/2008JA013524

Eastwood, J. P., Balogh, A., Dunlop, M. W., Horbury, T. S., & Dandouras, I. (2002). Cluster observations of fast magnetosonic waves in terrestrial foreshock. *Geophysical Research Letters*, *29*(22), 3-1–3-4. https://doi.org/10.1029/2002gl015582

Gary, P. S. (1985). Electromagnetic ion beam instabilities: Hot beams at interplanetary shocks. *The Astrophysical Journal*, *288*, 342–352. https://doi.org/10.1086/162797

Gary, P. S., Madland, C. D., Tsurutani, B. T., Goldstein, M. L., & Forslund, D. W. (1984). Electromagnetic ion instabilities: II. *Physics of Fluids*, *27*(7), 1852–1862. https://doi.org/10.1063/1.864797

Gary, S., Gosling, J. T., & Forslund, D. W. (1981). The electromagnetic ion beam instability upstream of the Earth's bow shock. *Journal of Geophysical Research*, *86*(A8), 6691–6696. https://doi.org/10.1029/ja086ia08p06691

Gary, S. P. (1986). Low-frequency waves in a high-beta collisionless plasma: Polarization, compressibility and helicity. *Journal of Plasma Physics*, *35*(3), 431–447. https://doi.org/10.1017/s0022377800011442

Gary, S. P. (1991). Electromagnetic ion/ion instabilities and their consequences in space plasmas—A review. *Space Science Reviews*, *56*(3–4), 373–415. https://doi.org/10.1007/BF00196632

Gary, S. P. (1992). The mirror and ion cyclotron anisotropy instabilities. *Journal of Geophysical Research*, *97*(A6), 8519–8529. https://doi.org/10.1029/92ja00299

Gary, S. P., Convery, P. D., Denton, R. E., Fuselier, S. A., & Anderson, B. J. (1994). Proton and helium cyclotron anisotropy instability thresholds in the magnetosheath. *Journal of Geophysical Research*, *99*(A4), 5915–5921. https://doi.org/10.1029/93ja03243

Gary, S. P., Montgomery, M. D., Feldman, W. C., & Forslund, D. W. (1976). Proton temperature anisotropy instabilities in the solar wind. *Journal of Geophysical Research*, *81*(7), 1241–1246. https://doi.org/10.1029/ja081i007p01241

Gary, S. P., & Tokar, R. L. (1985). The second-order theory of electromagnetic hot ion beam instabilities. *Journal of Geophysical Research*, *90*(A1), 65–72. https://doi.org/10.1029/ja090ia01p00065

Gary, S. P., & Winske, D. (1992). Correlation function ratios and the identification of space plasma instabilities. *Journal of Geophysical Research*, *97*(A3), 3103–3111. https://doi.org/10.1029/91JA02752

Gedalin, M. (2016). Transmitted, reflected, quasi-reflected, and multiply reflected ions in low-Mach number shocks. *Journal of Geophysical Research: Space Physics*, *121*(11), 10754–10767. https://doi.org/10.1002/2016JA023395

Gedalin, M., Dröge, W., & Kartavykh, Y. Y. (2016). Dependence of the spectrum of shock-accelerated ions on the dynamics at the shock crossing. *Physical Review Letters*, *117*(27), 275101. https://doi.org/10.1103/PhysRevLett.117.275101

Gosling, J. T., & Pizzo, V. J. (1999). Formation and evolution of corotating interaction regions and their three dimensional structure. In *Corotating interaction regions* (pp. 21–52). Springer.

Han, D.-S., Hietala, H., Chen, X.-C., Nishimura, Y., Lyons, L. R., Liu, J.-J., et al. (2017). Observational properties of dayside throat aurora and implications on the possible generation mechanisms. *Journal of Geophysical Research: Space Physics*, *122*(2), 1853–1870. https://doi.org/10.1002/2016JA023394

Han, D.-S., Nishimura, Y., Lyons, L. R., Hu, H.-Q., & Yang, H.-G. (2016). Throat aurora: The ionospheric signature of magnetosheath particles penetrating into the magnetosphere. *Geophysical Research Letters*, *43*(5), 1819–1827. https://doi.org/10.1002/2016GL068181

Hao, Y., Gao, X., Lu, Q., Huang, C., Wang, R., & Wang, S. (2017). Reformation of rippled quasi-parallel shocks: 2-D hybrid simulations. *Journal of Geophysical Research: Space Physics*, *122*(6), 6385–6396. https://doi.org/10.1002/2017JA024234

Hao, Y., Lembege, B., Lu, Q., & Guo, F. (2016a). Formation of downstream high-speed jets by a rippled nonstationary quasi-parallel shock: 2-D hybrid simulations. *Journal of Geophysical Research: Space Physics*, *121*(3), 2080–2094. https://doi.org/10.1002/2015JA021419

Hao, Y., Lu, Q., Gao, X., Huang, C., Lu, S., Shan, L., & Wang, S. (2014). He2+ dynamics and ion cyclotron waves in the downstream of quasi-perpendicular shocks: 2-D hybrid simulations. *Journal of Geophysical Research: Space Physics*, *119*(5), 3225–3236. https://doi.org/10.1002/2013JA019717

Hao, Y., Lu, Q., Gao, X., & Wang, S. (2016b). Ion dynamics at a rippled quasi-parallel shock: 2D hybrid simulations. *The Astrophysical Journal*, *823*(1), 7. https://doi.org/10.3847/0004-637x/823/1/7

Hao, Y. Q., Lu, D., Wu, X., & Liang (2023). Simulation dataset of "wave activities throughout a low-Mach number quasi-parallel shock: 2-D hybrid simulations" [Dataset]. Zenodo. https://doi.org/10.5281/ZENODO.7725025

Hao, Y. Q., Lu, D., Wu, S., Lu, L., Xiang, L., & Ke, Y. (2021). Low-frequency waves upstream of quasi-parallel shocks: Two-dimensional hybrid simulations. *The Astrophysical Journal*, *915*(1), 64. https://doi.org/10.3847/1538-4357/ac02ce

Hao, Y. X., Gao, Q., Lu, H., Wang, D., Wu, D., & Wang, S. (2018). Two-dimensional hybrid simulations of filamentary structures and kinetic slow waves downstream of a quasi-parallel shock. *The Astrophysical Journal*, *861*(1), 57. https://doi.org/10.3847/1538-4357/aacb2c

Hietala, H., Laitinen, T. V., Andreeova, K., Vainio, R., Vaivads, A., Palmroth, M., et al. (2009). Supermagnetosonic jets behind a collisionless quasiparallel shock. *Physical Review Letters*, *103*(24), 245001. https://doi.org/10.1103/PhysRevLett.103.245001

Hietala, H., Partamies, N., Laitinen, T. V., Clausen, L. B. N., Facsko, G., Vaivads, A., et al. (2012). Supermagnetosonic subsolar magnetosheath jets and their effects: From the solar wind to the ionospheric convection. *Annales de Geophysique*, *30*(1), 33–48. https://doi.org/10.5194/angeo-30-33-2012

Hoppe, M. M., & Russell, C. T. (1982). Particle acceleration at planetary bow shock waves. *Nature*, *295*(5844), 41–42. https://doi.org/10.1038/295041a0

Jarvinen, R., Alho, M., Kallio, E., & Pulkkinen, T. (2020). Ultra-low frequency waves in the ion foreshock of mercury: A global hybrid modeling study. *Monthly Notices of the Royal Astronomical Society*, *491*(3), 4147–4161. https://doi.org/10.1093/mnras/stz3257

Jian, L., Russell, C. T., Luhmann, J. G., & Skoug, R. M. (2006). Properties of stream interaction at one AU during 1995-2004. *Solar Physics*, *239*(1–2), 337–392. https://doi.org/10.1007/s11207-006-0132-3

Jones, F. C., & Ellison, D. C. (1991). The plasma physics of shock acceleration. *Space Science Reviews*, *58*(1), 259–346. https://doi.org/10.1007/bf01206003

Kajdič, P., Pfau-Kempf, Y., Turc, L., Dimmock, A. P., Palmroth, M., Takahashi, K., et al. (2021). ULF wave transmission across collisionless shocks: 2.5D local hybrid simulations. *Journal of Geophysical Research: Space Physics*, *126*(11), e2021JA029283. https://doi.org/10.1029/2021JA029283

Kan, J. R., & Swift, D. W. (1983). Structure of the quasi-parallel bow shock: Results of numerical simulations. *Journal of Geophysical Research*, *88*(A9), 6919–6925. https://doi.org/10.1029/ja088ia09p06919

Pfau-Kempf, Y., Battarbee, M., Ganse, U., Hoilijoki, S., Turc, L., von Alfthan, S., et al. (2018). On the importance of spatial and velocity resolution in the hybrid-Vlasov modeling of collisionless shocks. *Frontiers in Physics—Plasma Physics*, *6*, 44. https://doi.org/10.3389/fphy.2018.00044

Pfau-Kempf, Y., Hietala, H., Milan, S. E., Juusola, L., Hoilijoki, S., Ganse, U., et al. (2016). Evidence for transient, local ion foreshocks caused by dayside magnetopause reconnection. *Annales Geophysicae*, *34*(11), 943–959. https://doi.org/10.5194/angeo-34-943-2016

Pfau-Kempf, Y., Pokhotelov, D., Gutynska, O., Wilson, L. B., III, Walsh, B. M., von Alfthan, S., et al. (2015). Ion distributions in the Earth's foreshock: Hybrid-Vlasov simulation and THEMIS observations. *Journal of Geophysical Research: Space Physics*, *120*(5), 3684–3701. https://doi.org/10.1002/2014JA020519

Kennel, C. F., Edmiston, J. P., Scarf, F. L., Coroniti, F. V., Russell, C. T., Smith, E. J., et al. (1984a). Structure at the November 12, 1978, quasi-parallel interplanetary shock. *Journal of Geophysical Research*, *89*(A7), 5436. https://doi.org/10.1029/JA089iA07p05436

Kennel, C. F., Scarf, F. L., Coroniti, F. V., Russell, C. T., Wenzel, K. P., Sanderson, T. R., et al. (1984b). Plasma and energetic particle structure upstream of a quasi-parallel interplanetary shock. *Journal of Geophysical Research*, *89*(A7), 5419. https://doi.org/10.1029/JA089iA07p05419

Kilpua, E. K. J., Balogh, A., von Steiger, R., & Liu, Y. D. (2017). Geoeffective properties of solar transients and stream interaction regions. *Space Science Reviews*, *212*(3–4), 1271–1314. https://doi.org/10.1007/s11214-017-0411-3

Krauss-Varban, D. (1995). Waves associated with quasi-parallel shocks: Generation, mode conversion and implications. *Advances in Space Research. Proceedings of the D2.1 symposium of COSPAR scientific commission D*, *15*(8), 271–284. https://doi.org/10.1016/0273-1177(94)00107-c

Krauss-Varban, D., & Omidi, N. (1991). Structure of medium Mach number quasi-parallel shocks—Upstream and downstream waves. *Journal of Geophysical Research*, *96*(A10), 17715–17731. https://doi.org/10.1029/91ja01545

Krauss-Varban, D., & Omidi, N. (1993). Propagation characteristics of waves upstream and downstream of quasi-parallel shocks. *Geophysical Research Letters*, *20*(11), 1007–1010. https://doi.org/10.1029/93GL01125

Krauss-Varban, D., Omidi, N., & Quest, K. B. (1994). Mode properties of low-frequency waves: Kinetic theory versus Hall-MHD. *Journal of Geophysical Research*, *99*(A4), 5987–6009. https://doi.org/10.1029/93JA03202

Lee, K. H. (2017). Generation of parallel and quasi-perpendicular EMIC waves and mirror waves by fast magnetosonic shocks in the solar wind. *Journal of Geophysical Research: Space Physics*, *122*(7), 7307–7322. https://doi.org/10.1002/2017JA024340

Lee, K. H., & Lee, L. C. (2016). Generation of He+ and O+ EMIC waves by the bunch distribution of O+ ions associated with fast magnetosonic shocks in the magnetosphere. *Geophysical Research Letters*, *43*(18), 9406–9414. https://doi.org/10.1002/2016GL070465

Lembège, B., Giacalone, J., Scholer, M., Hada, T., Hoshino, M., Krasnoselskikh, V., et al. (2004). Selected problems in collisionless-shock physics. *Space Science Reviews*, *110*(3/4), 161–226. https://doi.org/10.1023/b:spac.0000023372.12232.b7

Leroy, M. M., Goodrich, C. C., Winske, D., Wu, C. S., & Papadopoulos, K. (1981). Simulation of a perpendicular bow shock. *Geophysical Research Letters*, *8*(12), 1269–1272. https://doi.org/10.1029/GL008i012p01269

Leroy, M. M., Winske, D., Goodrich, C. C., Wu, C. S., & Papadopolous, K. (1982). The structure of perpendicular bow shocks. *Journal of Geophysical Research*, *87*(A7), 5081–5094. https://doi.org/10.1029/JA087iA07p05081

Lin, Y. (2003). Global-scale simulation of foreshock structures at the quasiparallel bow shock. *Journal of Geophysical Research*, *108*(A11), 1390. https://doi.org/10.1029/2003JA009991

Lin, Y., Johnson, J. R., & Wang, X. Y. (2012). Three-dimensional mode conversion associated with kinetic Alfven waves. *Physical Review Letters*, *109*(12), 125003. https://doi.org/10.1103/PhysRevLett.109.125003

Lin, Y., & Wang, X. Y. (2005). Three-dimensional global hybrid simulation of dayside dynamics associated with the quasi-parallel bow shock. *Journal of Geophysical Research*, *110*(A12), A12216. https://doi.org/10.1029/2005JA011243

Lu, Q., Hu, Q., & Zank, G. P. (2009). The interaction of Alfven waves with perpendicular shocks. *The Astrophysical Journal*, *706*(1), 687–692. https://doi.org/10.1088/0004-637X/706/1/687

Lu, Q. M., & Wang, S. (2005). Formation of He2+ shell-like distributions downstream of the Earth's bow shock. *Geophysical Research Letters*, *32*(3), L03111. https://doi.org/10.1029/2004GL021508

Lu, Q. M., & Wang, S. (2006). Electromagnetic waves downstream of quasi-perpendicular shocks. *Journal of Geophysical Research*, *111*(A5), A05204. https://doi.org/10.1029/2005JA011319

Mandt, M. E., Kan, J. R., & Russell, C. T. (1986). Comparison of magnetic field structures in quasi-parallel interplanetary shocks: Observations versus simulations. *Journal of Geophysical Research*, *91*(A8), 8981–8985. https://doi.org/10.1029/JA091iA08p08981

McKean, M. E., Omidi, N., & Krauss-Varban, D. (1996). Magnetosheath dynamics downstream of low Mach number shocks. *Journal of Geophysical Research*, *101*(A9), 20013–20022. https://doi.org/10.1029/96JA01461

McKenzie, J. F., & Westphal, K. O. (1969). Transmission of Alfvén waves through the Earth's bow shock. *Planetary and Space Science*, *17*(5), 1029–1037. https://doi.org/10.1016/0032-0633(69)90107-x

Min, K., & Liu, K. (2015a). Fast magnetosonic waves driven by shell velocity distributions. *Journal of Geophysical Research: Space Physics*, *120*(4), 2739–2753. https://doi.org/10.1002/(ISSN)2169-9402

Min, K., & Liu, K. (2015b). Regime transition of ion Bernstein instability driven by ion shell velocity distributions. *Journal of Geophysical Research: Space Physics*, *120*(10), 8448–8454. https://doi.org/10.1002/2015JA021514

Narita, Y., & Marsch, E. (2015). Kinetic slow mode in the solar wind and its possible role in turbulence dissipation and ion heating. *The Astrophysical Journal*, *805*(1), 24. https://doi.org/10.1088/0004-637X/805/1/24

Omidi, N., Quest, K. B., & Winske, D. (1990). Low mach number parallel and quasi-parallel shocks. *Journal of Geophysical Research*, *95*(A12), 20717–20730. https://doi.org/10.1029/ja095ia12p20717

Otsuka, F., Matsukiyo, S., & Hada, T. (2019). PIC simulation of a quasi-parallel collisionless shock: Interaction between upstream waves and backstreaming ions. *High Energy Density Physics*, *33*, 100709. https://doi.org/10.1016/j.hedp.2019.100709

Palmroth, M., Archer, M., Vainio, R., Hietala, H., Pfau-Kempf, Y., Hoilijoki, S., et al. (2015). ULF foreshock under radial IMF: THEMIS observations and global kinetic simulation Vlasiator results compared. *Journal of Geophysical Research: Space Physics*, *120*(10), 8782–8789. https://doi.org/10.1002/2015JA021526

Palmroth, M., Raptis, S., Suni, J., Karlsson, T., Turc, L., Johlander, A., et al. (2021). Magnetosheath jet evolution as a function of life-time: Global hybrid-Vlasov simulations compared to mms observations. *Annales Geophysicae*, *39*(2), 289–308. https://doi.org/10.5194/angeo-39-289-202

Plaschke, F., Hietala, H., Blanco-Cano, X., Kajdič, P., Karlsson, T., Sibeck, D., et al. (2018). Jets downstream of collisionless shocks. *Space Science Reviews*, *214*(5), 81. https://doi.org/10.1007/s11214-018-0516-3

Quest, K. B., Forslund, D. W., Brackbill, J. U., & Lee, K. (1983). Collisionless dissipation processes in quasi-parallel shocks. *Geophysical Research Letters*, *10*(6), 471–474. https://doi.org/10.1029/GL010i006p00471

Richardson, I. G. (2018). Solar wind stream interaction regions throughout the heliosphere. *Living Reviews in Solar Physics*, *15*, 1. https://doi.org/10.1007/s41116-017-0011-z

Scholer, M. (1990). Diffuse ions at a quasi-parallel collisionless shock: Simulations. *Geophysical Research Letters*, *17*(11), 1821–1824. https://doi.org/10.1029/gl017i011p01821

Scholer, M. (1993). Upstream waves, shocklets, short large-amplitude magnetic structures and the cyclic behavior of oblique quasi-parallel collisionless shocks. *Journal of Geophysical Research*, *98*(A1), 47–57. https://doi.org/10.1029/92JA01875

Scholer, M., & Burgess, D. (1992). The role of upstream waves in supercritical quasi-parallel shock reformation. *Journal of Geophysical Research*, *97*(A6), 8319–8326. https://doi.org/10.1029/92ja00312

Scholer, M., & Fujimoto (1993). Low-Mach number quasi-parallel shocks' upstream waves. *Journal of Geophysical Research*, *98*(A9), 15275–15283. https://doi.org/10.1029/93JA01155

Scholer, M., Fujimoto, M., & Kucharek, H. (1993). Two-dimensional simulations of supercritical quasi-parallel shocks—Upstream waves, downstream waves and shock re-formation. *Journal of Geophysical Research*, *98*(A11), 18971–18984. https://doi.org/10.1029/93JA01647

Scholer, M., Kucharek, H., & Jayanti, V. (1997). Waves and turbulence in high Mach number nearly parallel collisionless shocks. *Journal of Geophysical Research*, *102*(A5), 9821–9834. https://doi.org/10.1029/97JA00345

Scholer, M., & Terasawa, T. (1990). Ion reflection and dissipation at quasi-parallel collisionless shocks. *Geophysical Research Letters*, *17*(2), 119–122. https://doi.org/10.1029/GL017i002p00119

Shan, L., Mazelle, C., Meziane, K., Delva, M., Lu, Q., Ge, Y. S., et al. (2016). Characteristics of quasi-monochromatic ULF waves in the Venusian foreshock. *Journal of Geophysical Research: Space Physics*, *121*(8), 7385–7397. https://doi.org/10.1002/2016JA022876

Shi, F., Lin, Y., & Wang, X. (2013). Global hybrid simulation of mode conversion at the dayside magnetopause. *Journal of Geophysical Research: Space Physics*, *118*(10), 6176–6187. https://doi.org/10.1002/jgra.5087

Su, Y., Lu, Q., Gao, X., Huang, C., & Wang, S. (2012). Ion dynamics at supercritical quasi-parallel shocks: Hybrid simulations. *Physics of Plasmas*, *19*(9), 092108. https://doi.org/10.1063/1.4752219

Su, Y., Lu, Q., Huang, C., Wu, M., Gao, X., & Wang, S. (2012b). Particle acceleration and generation of diffuse superthermal ions at a quasi-parallel collisionless shock: Hybrid simulations. *Journal of Geophysical Research*, *117*(A8), A08107. https://doi.org/10.1029/2012JA017736

Sun, J., Gao, X., Chen, L., Lu, Q., Tao, X., & Wang, S. (2016). A parametric study for the generation of ion Bernstein modes from a discrete spectrum to a continuous one in the inner magnetosphere. I. Linear theory. *Physics of Plasmas*, *2*, 022901. https://doi.org/10.1063/1.4941283

Sun, J., Gao, X., Lu, Q., Chen, L., Tao, X., & Wang, S. (2016). A parametric study for the generation of ion Bernstein modes from a discrete spectrum to a continuous one in the inner magnetosphere. II. Particle-in-cell simulations. *Physics of Plasmas*, *23*(2), 022902. https://doi.org/10.1063/1.4941284

Thomas, V. A., Winske, D., & Omidi, N. (1990). Reforming super-critical quasi-parallel shocks, 1. One- and two-dimensional simulations. *Journal of Geophysical Research*, *95*(A11), 18809–18819. https://doi.org/10.1029/JA095iA11p18809

Thomsen, M. F., Gosling, J. T., Onsager, T. G., & Russell, C. T. (1993). Ion and electron heating at the low-Mach-number, quasi-parallel bow shock. *Journal of Geophysical Research*, *98*(A3), 3875–3888. https://doi.org/10.1029/92JA02560

Turc, L., Ganse, U., Pfau-Kempf, Y., Hoilijoki, S., Battarbee, M., Juusola, L., et al. (2018). Foreshock properties at typical and enhanced interplanetary magnetic field strengths: Results from hybrid-Vlasov simulations. *Journal of Geophysical Research: Space Physics*, *123*(7), 5476–5493. https://doi.org/10.1029/2018JA025466

Turc, L., Roberts, O. W., Verscharen, D., Dimmock, A. P., Kajdič, P., Palmroth, M., et al. (2022). Transmission of foreshock waves through Earth's bow shock. *Nature Physics*, *19*(1), 78–86. https://doi.org/10.1038/s41567-022-01837-z

Wang, S., Chen, L.-J., Ng, J., Bessho, N., Le, G., Fung, S. F., et al. (2020). A case study of nonresonant mode 3-s ULF waves observed by MMS. *Journal of Geophysical Research: Space Physics*, *125*(11), e2020JA028557. https://doi.org/10.1029/2020JA028557

Wilson, L. B. (2016). Low frequency waves at and upstream of collisionless shocks. In *Washington DC American Geophysical Union Geophysical Monograph Series* (Vol. 216, pp. 269–291). https://doi.org/10.1002/9781119055006.ch16

Winske, D., & Leroy, M. (1984). Diffuse ions produced by electromagnetic ion beam instabilities. *Journal of Geophysical Research*, *89*(A5), 2673–2689. https://doi.org/10.1029/JA089iA05p02673

Xie, H. (2019). BO: A unified tool for plasma waves and instabilities analysis. *Computer Physics Communications*, *244*, 343–371. https://doi.org/10.1016/j.cpc.2019.06.014

Xie, H., & Xiao, Y. (2016). PDRK: A general kinetic dispersion relation solver for magnetized plasma. *Plasma Science and Technology*, *18*(2), 97–107. https://doi.org/10.1088/1009-0630/18/2/01

Yang, Z. W., Lembège, B., & Lu, Q. M. (2012). Impact of the rippling of a perpendicular shock front on ion dynamics. *Journal of Geophysical Research*, *117*(A7), A07222. https://doi.org/10.1029/2011JA017211

Yoon, P. H., & Fang, T.-M. (2008). Dispersion surfaces for low-frequency modes. *Plasma Physics and Controlled Fusion*, *55*(125), 002.

Zank, G. P., Li, G., Florinski, V., Hu, Q., Lario, D., & Smith, C. W. (2006). Particle acceleration at perpendicular shock waves: Model and observations. *Journal of Geophysical Research*, *111*(A6), A06108. https://doi.org/10.1029/2005JA011524

Zhang, H., Zong, Q., Connor, H., Delamere, P., Facsko, G., Han, D., et al. (2022). Dayside transient phenomena and their impact on the magnetosphere and ionosphere. *Space Science Reviews*, *218*(5), 1–146. https://doi.org/10.1007/s11214-021-00865-0

Zhao, J. (2015). Dispersion relations and polarizations of low-frequency waves in two-fluid plasmas. *Physics of Plasmas*, *22*(4), 89. https://doi.org/10.1063/1.4919257

Zhao, J. S., Voitenko, Y., Yu, M. Y., Lu, J. Y., & Wu, D. J. (2014). Properties of short-wavelength oblique Alfven and slow waves. *The Astrophysical Journal*, *793*(107), 12. https://doi.org/10.1088/0004-637X/793/2/107